PERGAMON International Journal of Multiphase Flow 25 (1999) 1645–1655

International Journal of Multiphase Flow

www.elsevier.com/locate/ijmulflow

Brief Communication

The flow characteristics of an interactive particle at low Reynolds numbers

R.C. Chen*, Y.N. Lu

Department of Mechanical and Marine Engineering, National Taiwan Ocean University, Keelung, Taiwan, ROC

Received 23 April 1998; received in revised form 27 November 1998

1. Introduction

There are many uses for multiphase flow systems in industrial processes. Knowledge of the interactive forces between different phases is crucial to the actual modeling and control of such systems. The drag force of a single particle in an infinite flow field depends on the surface properties of the particle and the flow conditions. Through either theoretical or experimental studies, certain effects on hydrodynamic behavior of a single sphere, including turbulence, vorticity, instability, historical force, virtual mass, etc., are understood. For those solid concentrations up to a certain level, the flow characteristics of an interactive particle become a strong function of the arrangement of surrounding particles. However, not too much is known about this point. It calls for the further investigation on the local drags and the flow structure of an interactive particle.

The first step is to understand the effects of the surrounding sphere arrangements on the local flow characteristics of an interactive sphere. Some of the early works are Rowe and Henwood (1961), Lee (1979) and Tsuji et al. (1982). All of them focused on the effects of inter-particle distances on the flow characteristics of an interactive sphere for $Re > 200$. For general industrial application, the particle Reynolds numbers (based on particle terminal velocity, diameter and fluid viscosity) are in the range 30–200. To study the flow properties of an interactive sphere in such a range of Reynolds number is therefore of great practical value. It should be also noted that the above-mentioned studies are all restricted to the case of two interacting spheres, no data are available for the sphere arrangements with more than three interactive spheres. Zhu et al. (1994) reported the measurements of drag forces of an interactive sphere for $Re < 200$. However, their work is still limited to the situation of only two

* Corresponding author. Tel: +886-2-462-2192; fax: +886-2-462-0836.
E-mail address: rcchen@newton.me.ntou.edu.tw (R.C. Chen)

PII: S0301-9322(98)00082-2

interactive spheres. Liang et al. (1996) concentrated their attention on the cases of multiple interactive spheres at a Reynolds number range between 30 and 106. However, no quantitative data and explanations of the wake flow structure relating to the change of drag forces were presented.

Obviously, the drag force of an interactive particle is strongly dependent on the instantaneous flow field around the particle. In another way, the surrounding flow structure turns out to be affected by the arrangement configuration of neighboring particles. Previous works are apparently incomplete. The objective of this study is to fill this hole and to provide both the basic picture for the further set-up of model and fundamental data for the numerical simulation.

2. Experiments

2.1. Drag force

The drag force of a sphere can be expressed as

$$F_{D0} = C_{D0}\frac{\pi}{8}\frac{\mu^2}{\rho}Re^2 \tag{1}$$

where F_{D0} is the particle drag, Re represents particle Reynolds number, C_{D0} is the drag coefficient and μ and ρ are the viscosity and the density of fluid, respectively. Glycerin/water mixture is chosen as the test liquid in an effort to reduce the experimental difficulty or uncertainty caused by the small magnitude of the drag itself. In the temperature range of 17–23°C, the viscosities of glycerin solution of 75–80 wt% are around 30–100 cp. For the Reynolds numbers ranging from 10 to 200, the drag forces for a sphere of 1–2 cm size will locate in a measurable range of the order from 10^{-3} to 10^{1} g in response to the augmentation of liquid viscosity. With the further help of a high-precision (of 1 mg resolution) electronic balance, the drag forces of an interactive sphere under low Reynolds numbers can be accurately measured. Fig. 1 shows the schematic diagram of test facility. The flow system is equipped with a cooling circulator to ensure the condition of constant temperature (i.e. constant viscosity). A viscosity meter of an accuracy of ± 1 cp is utilized to measure the viscosity of glycerin solution directly sampled from the circulating liquid during the test.

Stainless spheres of 1.6 cm diameter are adopted as the test spheres and experiments are conducted in a circular column of 15 cm ID and 150 cm high. The test sphere is connected, through a stainless rod of 0.1 cm diameter, to a stainless frame laid on the balance. Tests are conducted for spheres of the same size placed in different geometrical arrangements. All spheres, except the test one, are connected with rods one end of which are screwed to a specially designed plate. This plate is equipped with several rules of 1 mm accuracy to serve the purpose of precise three-dimensional alignment. Force measured by the electronic balance will consist of three components, namely, the gravitation, the buoyancy and the drags of both the sphere and the rod. The gravitational and buoyancy forces are measured before the flow is started. After measuring the drag of the sphere with the rod, the sphere is removed to leave the

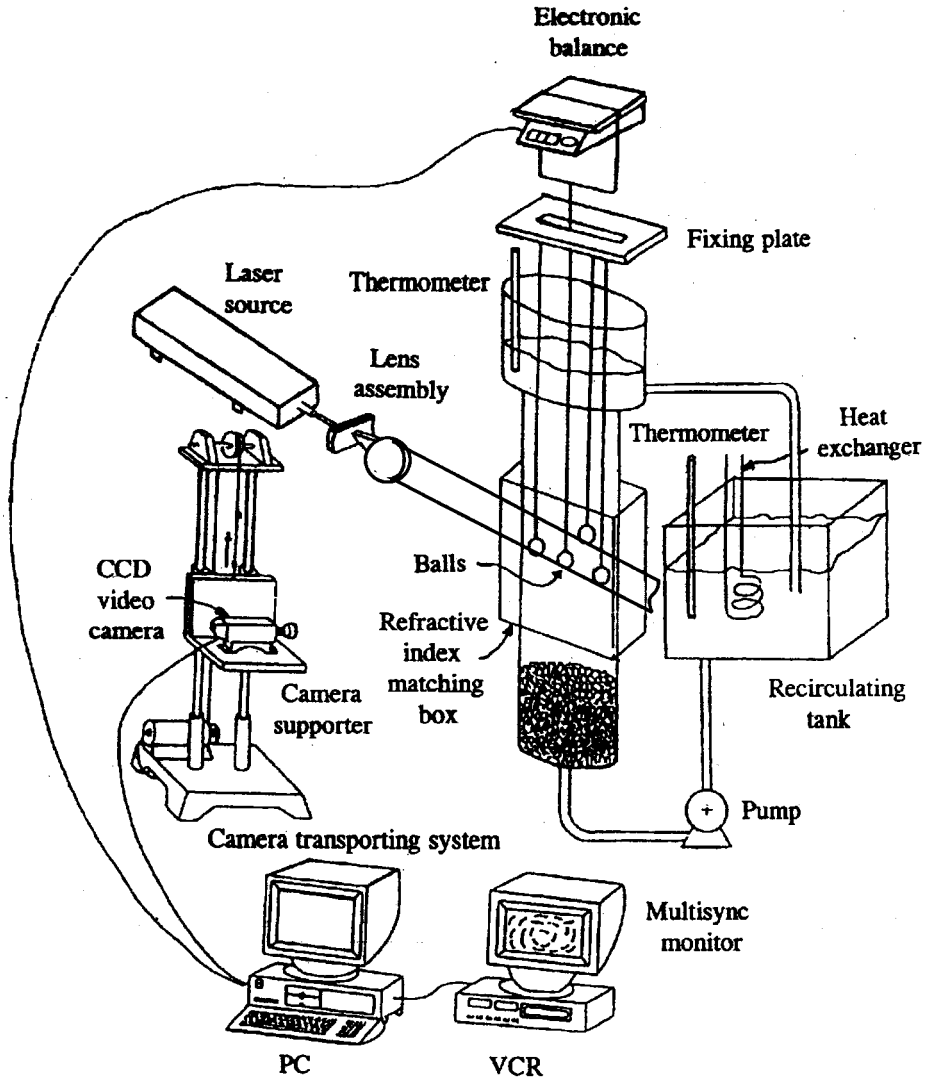

Fig. 1. Schematic diagram of the test facility.

rod. A sphere supported by an L type rod is then placed at the position just beneath but not touching the rod. In this way, one can truly measure drags of the rod under each sphere arrangement and Reynolds number. By eliminating the contributions from gravitation and buoyancy and the drag component of the rod, the drag of the sphere is obtained. Data presented in this work are the averaged results of 1000 measurements.

2.2. Flow structure

Particle image velocimetry (PIV) is applied to quantify the wake structure of interactive spheres. The two-dimensional flow field on a thin (2 mm) laser-sheet-illuminated area is

recorded by a CCD camera. A PIV interrogation program developed by Chen and Fan (1992) is utilized to identify seed particle images, locate centroids of particle images and compute displacement between image pairs. The instantaneous velocities are determined from the calculation of particle displacements in fields. There are many tiny bubbles inherently present in this highly viscous glycerin solution. Since most of those tiny bubbles are of less than 100 μm in size, the assumption of negligible slip velocity between each phase is approximately acceptable (Mei, 1997). A commercially available program, TECPLOT, is executed to post-process the PIV data. The primary velocity field (containing over 500 original velocity vectors) is interpolated using the Kriging algorithm (Davis, 1986) to a velocity field of 41×41 grid numbers. It should be noted that boundaries of both the sphere and the rod have been artificially set prior to the performance of interpolation.

Under the current field of view, each tiny bubble will occupy around one pixel and the uncertainty in locating the centroid can be reasonably estimated as $\pm 1/2$ pixel. Since most of the particle displacements detected are between 10 and 15 pixels, errors of velocity vectors are estimated to be less than 5%. Using the error analysis described by Davis (1986), the ratios between the standard errors and the interpolated velocities are between 10 and 15%.

3. Results and discussion

3.1. Two spheres aligned streamwise

PIV results indicate that both the length and the width of the wake region of the trailing sphere are significantly reduced when two spheres are in contact. The flow visualization shows that the occurrence of separation for the trailing sphere is delayed for more than 10° when $l/d = 0$. It leads to the recovery of back pressure and consequently a decrease in the form drag. The total drag is however reduced to be only 20% of that of a non-interactive sphere, as demonstrated in Fig. 2, which gives the drag coefficients of the trailing sphere with relations to the Reynolds numbers and the dimensionless inter-particle distances l/d (defined as the shortest distance l between sphere surfaces divided by the particle diameter d). Since the form drag occupies only a small part of the total drag at such low Reynolds numbers, the tremendous reduction in the total drag should be primarily contributed from the decrease in the friction drag. Through the examination of flow visualization pictures, a liquid nearly-stagnation region is identified near the area where both spheres make contact. In the meantime, the wake of the leading sphere is observed to be suppressed to an infinite set of ring vortices nested toward this liquid nearly-stagnant region as shown and described by Taneda (1979). Liquid from these infinite sequences of vortex rings is moving in a relatively slow manner and is isolated from the free stream. Apparently, the significant decrease in the drag is mainly caused by the nature of this slow-moving vortical flow structure and the existence of a liquid nearly-stagnant region near the front surface of the trailing sphere. Due to the influence of the suppressed wake of the leading sphere, fluid near the trailing sphere's front surface will have a much lower velocity and pressure gradient. The occurrence of separation can therefore be delayed. A reduction in the size and the strength of wake region consequently results. This effect is most pronounced at $l/d = 0$. As the inter-particle distance increases, the fluid has both the time and the space to

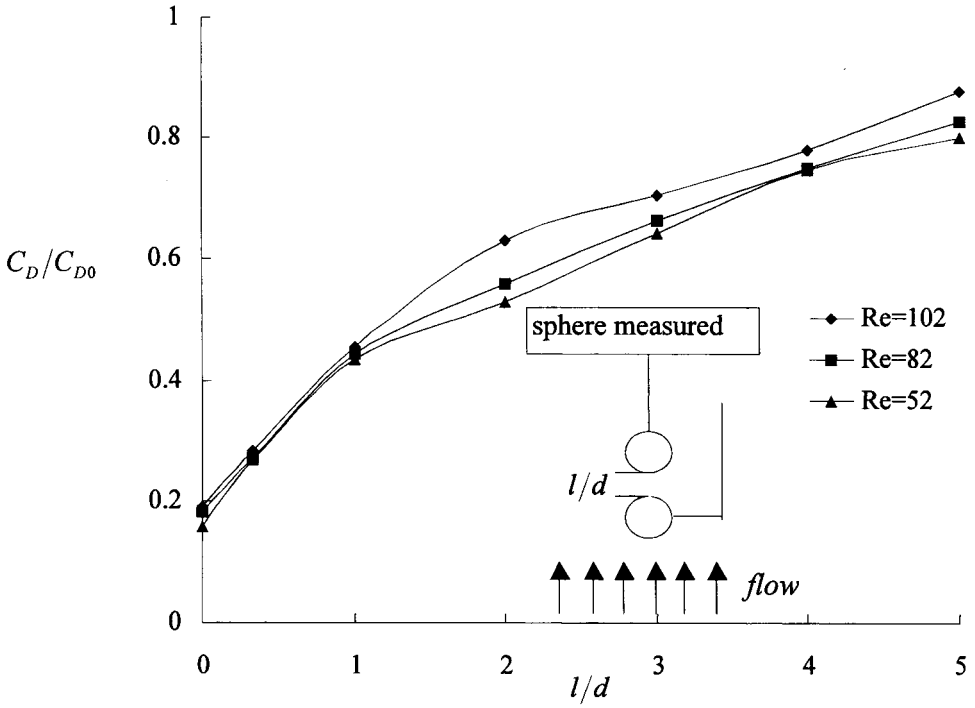

Fig. 2. Drag coefficients of the trailing sphere for two spheres aligned streamwise.

retain its velocity. Therefore, the delay of separation caused by the influence of the wake of the leading sphere is promptly attenuated as l/d increases.

At $l/d = 1/3$, wake of the leading sphere is still suppressed by the trailing sphere. However, the size of the above-mentioned liquid nearly-stagnant region has been substantially decreased. This results in a rapid recovery of the drag. As the inter-particle distance is increased to one diameter, the wake of the leading sphere is still under suppressed. However, different from the cases at $l/d = 0$ and $1/3$, the fluid is observed to flow through the gap between two spheres in a random and turbulent manner. The penetration of fluid stream through the inter-particle gap not only makes the existence of the liquid nearly-stagnant region impossible, but also induces a large measurement uncertainty. The total drag is rapidly recovered in response to the collapse of the liquid nearly-stagnant region. After this has occurred, the recovering rate of drag suddenly drops. At $l/d = 2$, the vortical wake structure of the leading sphere becomes identifiable in spite of the fact that it appears to be an asymmetrical open type under the influence of the trailing sphere. For $l/d > 2$, a closed wake emerges behind the leading sphere. In addition, the trailing sphere is now located outside the wake region of the leading sphere and therefore the direct impact of the wake of the leading sphere on the trailing sphere becomes less insignificant. Therefore, from now on, the progressive reformation of drag is mainly due to the gradual reduction in the indirect influence of the wake of the leading sphere.

By extrapolating Fig. 2 it is shown the trailing sphere cannot fully eliminate the influence of the leading sphere until $l/d \geqslant 10$. This finding agrees well with the work of Rowe and Henwood (1961). The interactive influence of the leading sphere on the trailing sphere diminishes as

Reynolds numbers increased. However, the effect of Reynolds number is not prominent for $l/d \leqslant 1$. This result gives an indirect support for the existence of both the slowly moving vortical flow structure and a liquid nearly-stagnant region near the contact surface of spheres, and these being the major causes of the significant decrease in drag for $l/d \leqslant 1$. After the liquid nearly-stagnant region collapses, the influence of Reynolds number on the drag reduction becomes visible. Apparently, the drag reduction attenuates at higher Reynolds numbers.

3.2. Two spheres aligned side by side

Since the flow is not symmetrical to the sphere's centerline, the wake structure is asymmetrical and the sphere is observed to conduct a minor swing motion. This swinging motion makes the drag measurements at $l/d = 0$ impossible due to the occurrence of unallowable uncertainty. Wake size is larger than that of a non-interactive sphere and is decreased with the increase in the inter-particle distance. The increase in wake size may be caused by the "nozzle effect" arising from fluid passing through the small gap between two spheres. The nozzle effect will result in an increase in the local Reynolds numbers. Consequently the form drag is increased through the early occurrence of separation and the friction drag is also augmented through the increase in the velocity gradient near the sphere wall. This nozzle effect is immediately attenuated as the inter-particle distance is extended to one diameter. The sudden decrease in the length of the wake region truly reflects the fact.

The recovery of drag shares the same tendency of the wake size as that clearly shown in Fig. 3. Basically, two drag augmentation rates can be identified. The appearance and vanishing of the nozzle effect is responsible for the above finding. Based on the heavy overlap of curves in Fig. 3, the Reynolds number effect seems not to play a significant role in the determination of the interactive drag forces. From the extrapolation of curves in Fig. 3 one finds that the sphere will be free of interaction for $l/d \geqslant 4$. By comparing with the results under the condition of two spheres placed streamwise, one knows that the magnitudes of the change of drag forces are smaller and the distance free of interaction is shorter. It can be concluded that the influence of a longitudinally placed sphere is dominant to that of a laterally placed sphere.

3.3. Three spheres aligned side by side

Flow characteristics of the center sphere when it suffers from interactions of two side-by-side spheres are shown in Figs. 4 and 5. Under the condition that one of the inter-particle distances is fixed at $l/d = 1/3$, the wake region located in the side of larger inter-particle distance is dilated with vortex centers being shifted away from the supporting rod. The dilation of wake region and the shift of vortex centers are not so apparent when spheres on both sides are placed at the same inter-particle distance ($l/d = 1/3$ here). However, the shift of wake centers becomes obvious when the inter-particle distances are uneven. Basically, although small difference exists, wake sizes on both the sides with and without sphere nearby are similar when the sphere only interacts with one side sphere. For the sphere interacting simultaneously with two side-by-side spheres, wake size on the side with a greater l/d ($> 1/3$) is always larger than that on the side with $l/d = 1/3$, as shown in Fig. 4. In addition, because of the nozzle effect, the wake starts to become open as one can observe the free stream is entrained from the right

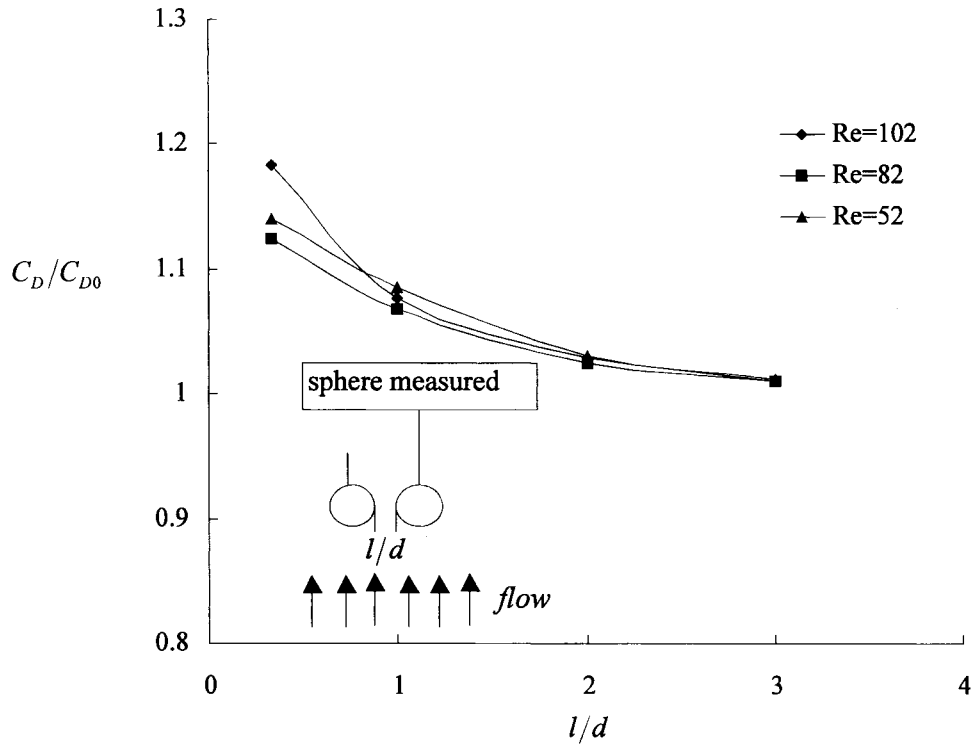

Fig. 3. Drag coefficients for two spheres aligned side by side.

to the left (the side with larger l/d). The entrainment of the free stream not only causes the dilation of wake region and the shift of vortex centers, but also highly enhances the three-dimensional flow pattern. It should be noted that the phenomena of free stream entrainment are not so obvious when the sphere interacts with only one side sphere. It is noted from Fig. 5 that drags are increased in response to the additional interaction with this extra sphere placed at $l/d = 1/3$ on the other side of test sphere. The increase in the local Reynolds numbers due to the nozzle effect explained above should be principally responsible for the augmentation of drags. Again, the Reynolds number effect seems minor.

3.4. Three spheres aligned in a reversed L manner

Fig. 6 shows the change of drag coefficients with the Reynolds numbers and the longitudinal inter-particle distances under the influence of a side sphere located at $l/d = 1/3$ when three spheres are aligned in a reversed L manner. The trends of drag recovery in both Figs. 2 and 6 are similar. However, magnitudes of the drag reduced in Fig. 6 are smaller than those in Fig. 2. This fact is due to the drag augmentation resulting from the extra interaction with a side sphere. Especially, for $l/d \leqslant 1$, the drag magnitudes reduced are substantially recovered under the interactive influence of a side sphere. It implies that there may exist a certain nonlinear imposing relation between each other. For $l/d \leqslant 1$, it remains to find such nonlinear relations. However, for $l/d > 1$, it is interesting to note that the drag coefficients in Fig. 6 equal

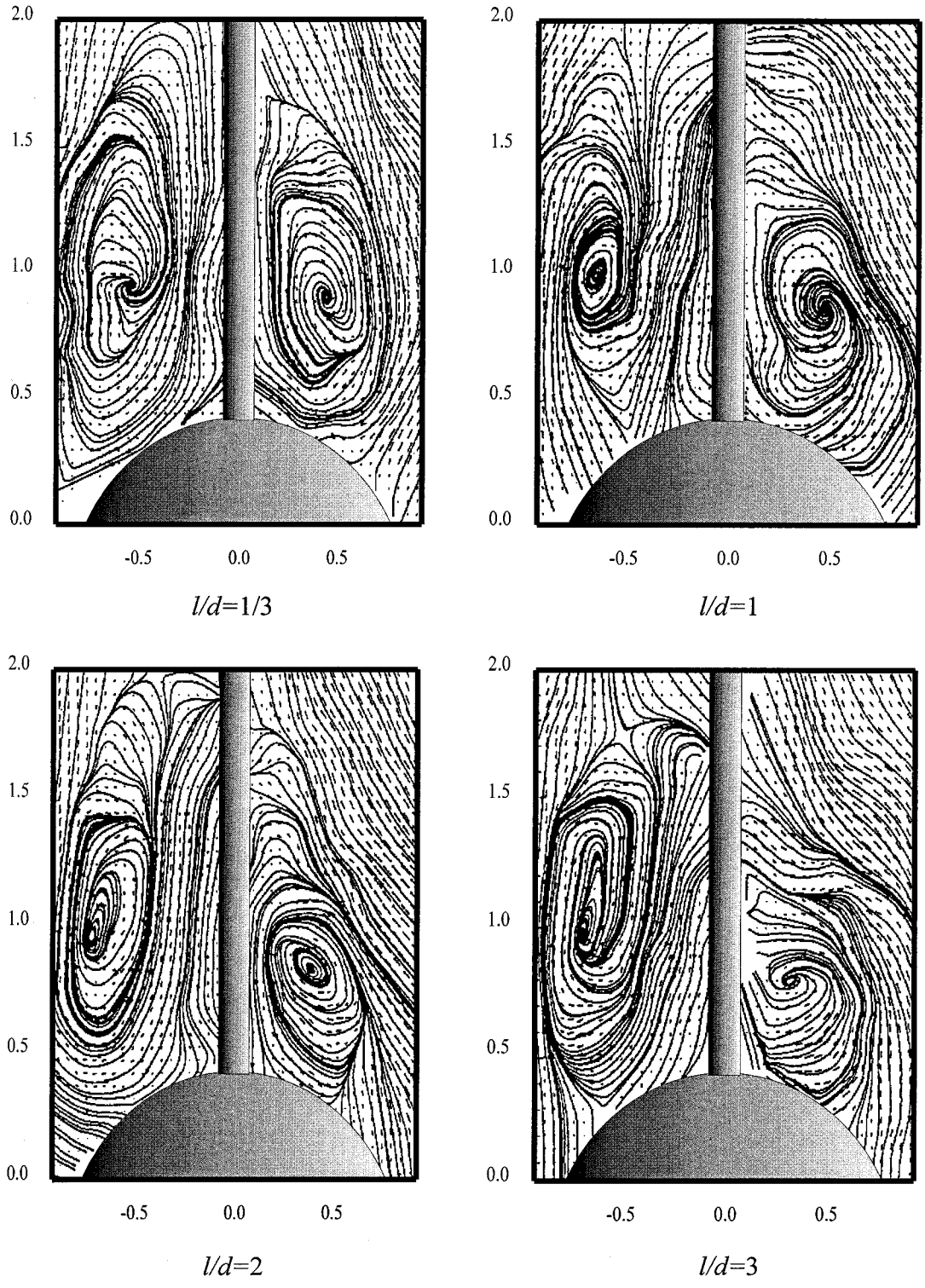

Fig. 4. Velocity fields with integrated streamlines of the wake region for three spheres aligned side by side.

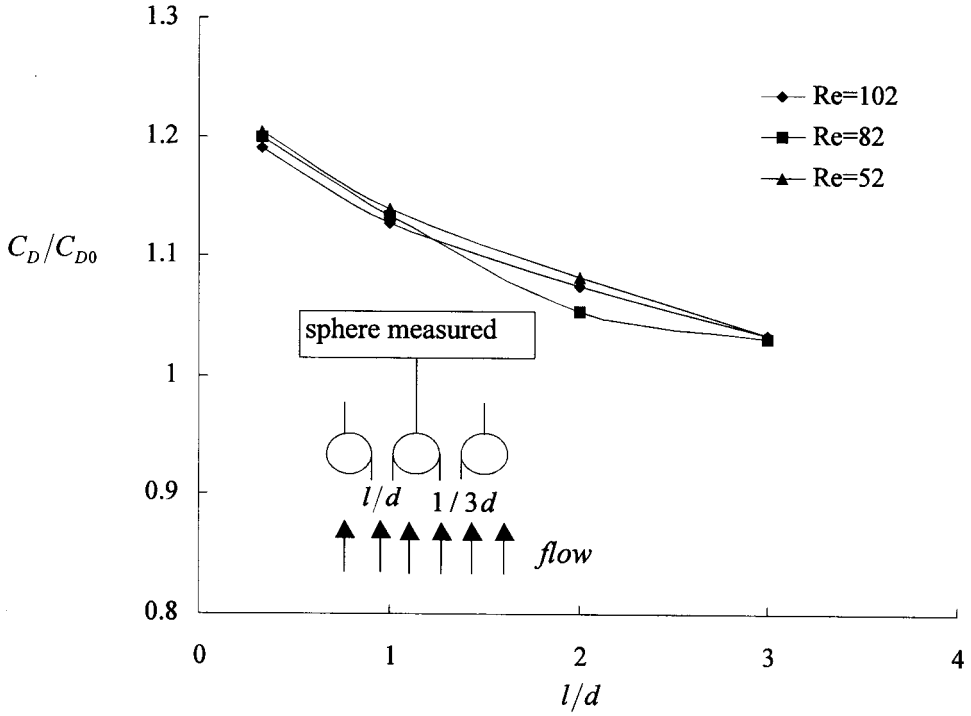

Fig. 5. Drag coefficients for three spheres aligned side by side.

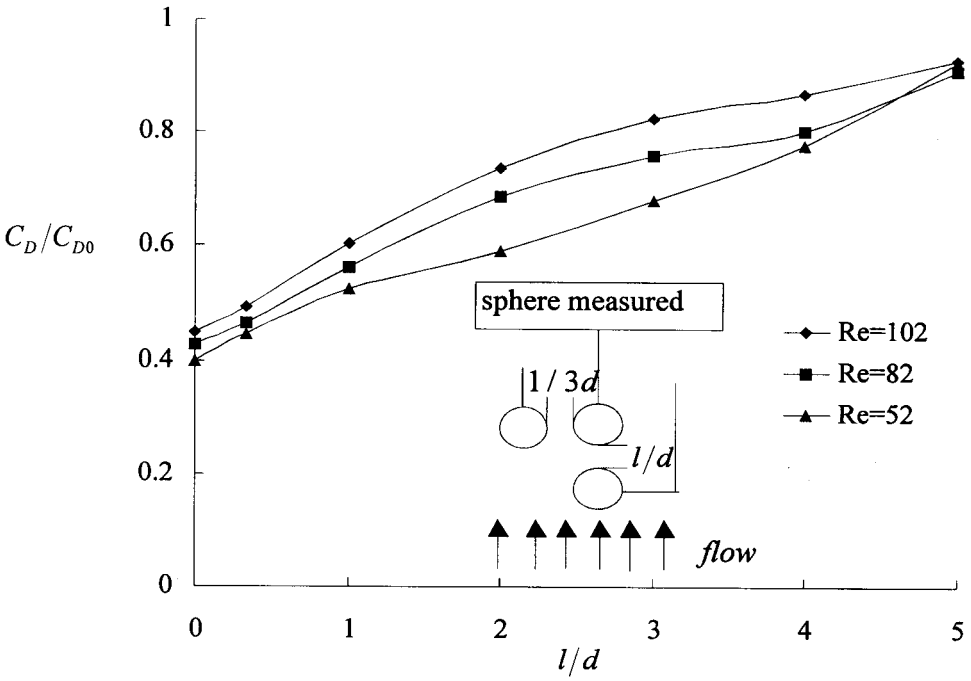

Fig. 6. Drag coefficients for three spheres aligned in a reversed L manner.

approximately to the products of drag coefficients in Figs. 2 and 4 (at $l/d = 1/3$). The averaged errors are within an amazing range of $\pm 5\%$.

Recall that, when two spheres are aligned streamwise, the existence of a liquid nearly-stagnant region and the impact of compressed wake flow of the leading sphere are the major two reasons for the tremendous reduction of the friction drag of the trailing sphere for $l/d \leqslant 1$. This liquid nearly-stagnant region is visualized to be almost destroyed and the slow-moving compressed vortical flow is apparently speeded up under the current condition. This observation explains why the friction drag and consequently the total drag are greatly recovered for $l/d \leqslant 1$ when compared with those in Fig. 2. The liquid nearly-stagnant region again disappears for $l/d > 1$. The Reynolds number effect on the drag force is similar to that shown in and explained for Fig. 2.

4. Concluding remarks

The drag and the fluid mechanic characteristics of an interactive sphere at particle Reynolds numbers less than 200 have been studied. The size of the wake region of the trailing sphere is greatly reduced under the influence of the leading sphere when two spheres are aligned streamwise. The influence of the wake of the leading sphere and the existence of a liquid nearly-stagnant region located at the gap between two streamwise-placed spheres cause the extreme reduction in the total drag. Drag is increased due to the increase in local Reynolds numbers caused by the nozzle effect when two spheres are aligned side by side. However, the influence is limited and the drag increase is minor compared with the case of two spheres aligned streamwise. When three spheres are aligned side by side, for the center sphere, the wake size is enlarged and the vortex centers of wake are laterally shifted away from the rod as the flow becomes three dimensional. Study of three spheres aligned in a reversed L manner shows that the drag coefficients of the trailing sphere are the products of those values at the corresponding inter-particle distance when the sphere is influenced by the leading particle and by the side sphere alone.

Acknowledgements

This work was financially supported by the National Science Council, Republic of China under contract no. 85-2611-E-019-019.

References

Chen, R.C., Fan, L-S., 1992. Particle image velocimetry for characterizing the flow structure in three-dimensional gas–liquid–solid fluidized beds. Chem. Engng. Sci. 47, 3615–3622.

Davis, J.C., 1986. Statistics and data analysis in geology. Wiley, New York.

Lee, K.C., 1979. Aerodynamic interaction between two spheres at Reynolds numbers around 10^4. Aero. Q. 30, 371–385.

Liang, S.C., Hong, T., Fan, L-S., 1996. Effects of particle arrangements on the drag force of a particle in the intermediate flow regime. Int. J. Multiphase Flow 22, 285–306.

Mei, R., 1997. Velocity fidelity of flow tracer particles. Exp. Fluids 22, 1–13.

Rowe, P.N., Henwood, G.A., 1961. Drag forces in hydraulic model of a fluidised bed—part I. Trans. Inst. Chem. Engrs 39, 43–54.

Taneda, S., 1979. Visualization of separating Stokes flows. J. Phys. Soc. Jpn 46, 1935–1942.

Tsuji, Y., Morikawa, Y., Terashima, K., 1982. Fluid-dynamic interaction between two spheres. Int. J. Multiphase Flow 8, 71–82.

Zhu, C., Liang, S.C., Fan, L-S., 1994. Particle wake effects on the drag force of an interactive particle. Int. J. Multiphase Flow 20, 117–129.